Journal of Science and Technology
ISSN: 2456-5660, Volume 6, Issue 6 (NOV-DEC 2021)

www.jst.org.in DOI: https://doi.org/10.46243/jst.2021.v6.i6.pp19-30

The Osteogenic Potential of Titanium Dioxide Nanoparticles of Different Sizes and Shapes.

Dr.A.Padmanabham[1],Mr.V.N.V.Radha Kishna Murty[2],
Associate Professor[1,2],
Mail Id:apnabham@gmail.com,Mail Id:radhakrishna.veluri@gmail.com,
Department of Physics,
DNR College of Engineering and Technology,
Bhimavaram,
B.V.Raju College of Engineering and Technology,Vishnupur,
Bhimavaram,

To Cite this Article

*Dr.A.Padmanabham ,Mr.V.N.V.Radha Kishna Murty"**The Osteogenic Potential of Titanium Dioxide Nanoparticles of Different Sizes and Shapes**", Journal of Science and Technology, Vol.6, Issue 6, NOV-DEC 2021, pp.:19-30.*

Article Info

Received: 18-11-2021 Revised: 24-11-2021 Accepted: 01-12-2021 Published: 10-12-2021

Introduction

For example, nanoparticles (NPs) are increasingly being used in healthcare, antimicrobial materials, optical and electrical devices, and medication delivery systems [1, 2]. NPs have a greater specific surface area than tiny particles, which increases their reactivity, making them more attractive to researchers. Nanoparticle bioactivity is considered distinct from that of its fine-size equivalent because of surface features such as energy level, electronic structure and reactivity [3]. As a result, several studies [4–10] have examined the possible effects of NPs on cells and tissue. Because TiO2 NPs are NPs, they have the same surface characteristics as the rest of the NPs. TiO2 NPs are extensively employed as a photocatalyst in solar cells, a pigment in paints, a corrosion-protective coating on bone implants, and more because of their unique physicochemical features [11–14]. TiO2 NPs have recently come under scrutiny for their potential impact on human health. A study by Ferin et al. [15] found that ultrafine TiO2 (20 nm) reached the pulmonary interstitium in the rat lung and produced inflammation compared to fine TiO2 at the same mass burden. In vitro and in vivo, Kumazawa et al. [16] found that neutrophils phagocytized Ti par ticles (1-3 m) and concluded that the cytotoxicity of Ti particles was size dependant. After then, TiO2 NPs have been extensively studied to identify their potential toxicity to different cells, including human fibroblasts, macrophages, and cutaneous microvascular endothelial cells [17, 18]. Particle sizes, surface coatings, crystal shapes, and dosages were all used in these research to highlight the cell toxicological effects of TiO2 NPs. It is unknown how TiO2 NPs affect osteogenic differentiation in cells. The human body's bone tissue is one of the most active and versatile types of tissue there is. Trauma, damage, infection, and loss of bone extracellular matrix are among the most serious health threats to humans [22]. [23] Bone tissue engineering is a novel strategy to repairing bone abnormalities and designing bone tissue transplantation. It's been shown in several research on bone tissue engineering that a variety of materials, stress or other variables may impact bone tissue cell proliferation, differentiation or mineralization. Osteoblasts, in particular, populate the bone defect during bone repair. It is the Golgi apparatus of osteoblasts that allows them to release a huge number of proteins onto the surface of the bone matrix [34]. Research into whether or not TiO2 NPs may promote osteogenic differentiation in cells is significant since osteoblasts are critical in bone production. By coculturing MC3T3-E1 cells with TiO2 NPs, we investigated how the concentration, shape, and size of NPs affected the proliferation and osteogenic differentiation of preosteoblasts. The CCK-8 kit is used to monitor MC3T3-E1 cell proliferation. Flow cytometry is used to study cell death and reactive oxidative species (ROS). Analysis of ALP, OCN, and Alizarin Red staining of mineralized osteoblast nodules helps determine the differentiation and proliferation of osteoblasts.

Materials and Methods

In this investigation, R2 (Wan Jing New Material Co. Ltd.; purity > 99:8 percent) and rutile TiO2 NPs (A2; Beijing Nanchen Technology Develop ment Co. Ltd.) without any coating were utilised. It was bought from Gibco Invitrogen's Minimum Essential Medium Eagle (MEM) (USA). MDgenics supplied the foetal bovine serum (FBS)

www.jst.org.in DOI: https://doi.org/10.46243/jst.2021.v6.i6.pp19-30

(New Zealand). INALCO supplied penicillin G and streptomycin for use in this study (USA). Beyotime Institute of Biotechnology provided the cell counting kit-8 (CCK-8), ALP assay kit, 2,7-dichlorodihydrofluorescein diacetate (DCFH-DA), total glutathione assay kit, total superoxide dismutase (SOD) assay kit with WST-1, lipid peroxidation product (malondialdehyde, MDA) assay kit, cell lysis buffer, and BCA protein assay kit (Jiangsu, China). Roche Co. Ltd. provided phenylmethanesulfonyl fluoride (PMSF). AMRESCO supplied the trypsin (USA). Nanjing Jiancheng Bioengineering Institute supplied the mouse bone gla protein/osteocalcin (BGP/OCN) ELISA kit. Bellancom Chemistry provided the company with Alizarin Red S. To get dexamethasone and -glycerophosphate, we went to Sigma-Fluka. AMRESCO bought L-ascorbic acid (USA). For the remainder of this experiment, only analytical-grade chemicals were employed. In anhydrous ethanol, TiO2 NPs were suspended and ultrasonically agitated at 200 watts for 5 seconds ten times. The silicon wafer was dipped into the suspension. SEM revealed the TiO2 NPs' size and form (Hitachi S-4800 SEM). The structural profile of TiO2 NPs was characterised by TEM (FEI Tecnai G2 F20 S Twin). Quanta chrome Instruments, USA, used the Quadrasorb SI analyzer (N2 absorption at 77.3 K) to measure the surface parameters of TiO2 NPs, such as the surface area, average pore diameter, and pore volume. An analyzer that measures particle size and zeta potential was used to determine the dispersion and aggregation of TiO2 NPs in aqueous solution (Zetasizer Nano ZS90, Malvern Instruments, UK). Suspended PBS-TiO2 NPs Sedimentary Observations The sediment of the TiO2 NP suspension was studied in a series of studies. Fresh sterilised PBS solution was used to disseminate the TiO2 NPs at the following concentrations: 10, 30, and 100 g/mL each. TiO2 NPs were dispersed by ultrasonicating the sus pension for 5 s at 200W for 10 times (ultrasonic cell disruptor system, Jiangsu, China). After that, the suspension of TiO2 NP was permitted to stand for 12 hours. A digital camera was used to document the sediment's current condition (Canon PowerShot S95, Japan). For the next step, PBS was used to create nano-TiO2 suspensions containing 5, 10, 20, and 30 ng/mL of TiO2. In order to improve NP dispersion, 2 mg/mL bovine serum albumin (BSA) was added to PBS (40 : 1 compared with the weight of TiO2 NPs). As a counterpoint, MEM was infused with TiO2 NPs at a concentration of 20 g/mL. After a 48-hour period, all TiO2 NP suspensions were analysed for sediment. Cultivation of cells (section 2.4). The National Platform of Experimental Cell Resources for Science and Technology provided the MC3T3-E1 mouse preosteoblast cells (Beijing, China). The cells were incubated at 37°C in a humidified environment containing 5% CO2 in MEM supplemented with 10% FBS, 100 U/mL penicillin, and 100 g/mL streptomycin. When the cells achieved 80% to 100% confluence, the culture media was replaced every three days. A density of 8:0 103 cells per well in 100 L culture media was used to measure cell activity in the 96-well plates. Seeding cells at a density of 2/5 105 cells/well in culture media was used for further investigations, which took place in 6-well plates. The cells were treated to four different nano-TiO2 suspensions after they had reached 70% confluence. BSA was added to a PBS solution containing the TiO2 NP suspension (1mg/mL). Ultrasonication was performed for 30 minutes to prevent agglomeration of the suspensions. MEM was used to dilute the suspension to a concentration of 20 ng/mL. When 10% FBS was added, the TiO2 NP suspension had a concentration of 20 ng/mL.

Table 1: Characterization of TiO_2 NPs.

Original no.	No.	Crystal	Shape	Size (nm)	Specific surface area (m^2/g)	Average pore diameter (nm)	Total pore volume (cc/g)	Z-Ave (d·nm)	Zeta potential (mV)
1	A1	Anatase	Red blood cell like	D: 45.87 ± 7.75	97.75	1.79	0.56	166.6	5.7
6	A2	Anatase	Sphere	D: 79.39 ± 22.58	10.37	1.93	0.05	653.3	-18.7
2	R1	Rutile	Long rod	D: 52.37 ± 7.35 L: 86.55 ± 12.13	21.51	2.17	0.22	408.7	2.3
4	R2	Rutile	Long rod	D: 25.46 ± 9.65 L: 75.34 ± 13.28	28.27	2.44	0.17	183.6	-22.0

used MC3T3-E1 cells as a culture medium. In each experiment, the control was culture medium without TiO2 NPs. 2.5. The CCK-8 Assay is performed. We used a concentration of NPs of 20 g/mL on MC3T3-E1 cells exposed for 24 hours to four different varieties of nano-TiO2. A second round of washing with PBS was followed by incubation with 100 L MEM and 10 L CCK-8 for 2 h, at 37°C. The negative control was MEM and CCK-8 without cells. Microplate reader Varioskan Flash (3001, USA) was used to measure the intensity at 450 nm. As a proportion of viable cells, cell viability was measured. All trials were carried out in at least three separate instances. 2.6. Measurement of ROS and Superoxide Production. In order to measure ROS generation, DCFH-DA fluorescence was used. MC3T3-E1 cells were collected after 24 hours of coculture with four kinds of 20 g/mL TiO2 NPs. In order to verify that the probe had a complete response with the cells, the cells were treated with 10 M DCFH DA in the dark for 20 minutes at 37° C and reverse mixed every 3–5 minutes. After that, the cells were rinsed three times

www.jst.org.in DOI: https://doi.org/10.46243/jst.2021.v6.i6.pp19-30

using a serum-free media. A positive control was performed using cells that had been grown with 1 L of Rosup. Fluorescent chemical 2′,7′-dichlorofluorescein (DCF) is produced via ROS-induced oxidation of DCFH (BD FACSCalibur, USA). DCF fluorescence was measured using 20,000 cells in each experiment group that were excited at 488 nm and emitted at 530 nm. In the presence of superoxide, WST-1 was reduced to an orange soluble formazan that could be read at 450 nm. Catalase and SOD were employed in this kit to ensure that H2O2 was not interrupted, and the results were corrected. MC3T3-E1 Cells were examined by TEM. MC3T3-E1 cells cocultured with or without TiO2 NPs were scraped and immediately submerged in 2.5 percent glutaraldehyde overnight at 4° C for the TEM examination. Using PBS as a pre-treatment, the samples were fixed with 1 percent osmium tetroxide before being dehydrated in a succession of ethanols, embedded in araldite, and polymerized for 24 hours at 37 degrees Celsius. We used a Hitachi H-600 TEM (Japan) with the Cell Apoptosis Assay to examine the ultra-thin sections (60nm) stained with uranyl acetate and lead citrate. By using Annexin V-FITC and PI assays, as well as flow cytometric analyses, apoptosis was determined. The detection kit's instructions on how to use Annexin V-FITC/PI were strictly followed. A concentration of 20 g/mL of TiO2 NPs was applied to the cultured cells for 24 hours. Trypsinization was used to extract cells, which were rinsed with PBS, then centrifuged for 5 minutes at 1,000 rpm. Finally, the cells were resuspended in Annexin V binding buffer solution at a concentration of 1 106 cells/mL. A 5 L aliquot of Annexin V-FITC was incubated with 100 L of cells in a tube for 15 minutes at room temperature and in the dark. Necrotic cells may be identified by the presence of the dye PI. Flow cytometry was used to evaluate the cells after just one hour of labelling, and 400 L binding buffer was added to each tube. Assessment of ALP and OCN activity. In the alkaline buffer, p-nitrophenol was released from p-nitrophenyl phosphate (pNPP). After three PBS washes, cell layers on a 6-well plate were treated for 40 minutes on ice with 100 L of cell lysis buffer containing 1 percent Triton X-100. An EP tube was used to collect the cell lysates using a cell scraper. Following a 10-minute centrifugation at 12,000 rpm at 4°C, the supernatant was utilised to measure activity of the enzyme. In addition, the BCA technique was used to determine the protein concentration. ELISA was used to determine the concentration of OCN products in the culture medium. According to the manufacturer's instructions, the tests were carried out exactly as specified. An ELISA microplate was coated with a purified anti-mouse OCN antibody. The lyophilized culture medium was reconstituted in PBS and pipetted into the wells, which were then incubated. Each

www.jst.org.in DOI: https://doi.org/10.46243/jst.2021.v6.i6.pp19-30

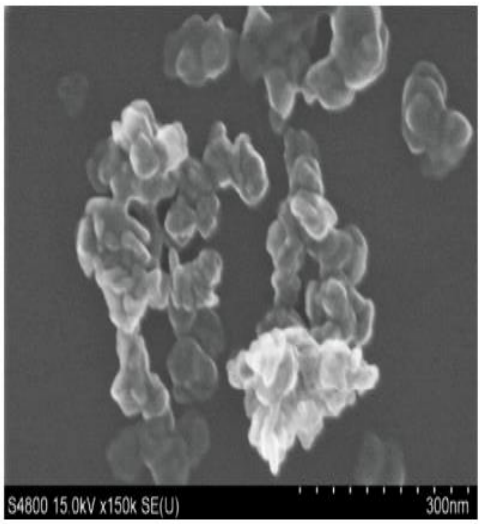

(a)

and every one of the OCN present had to abide by the

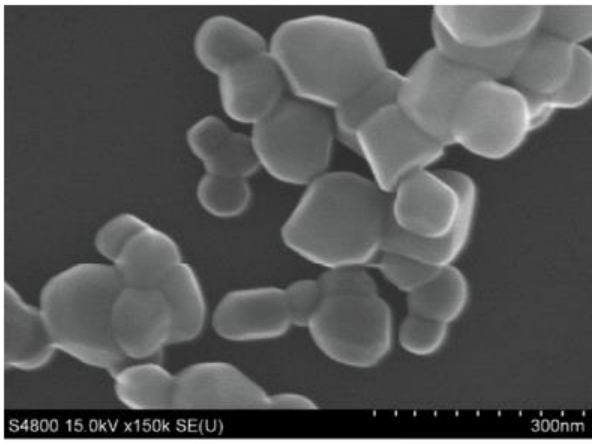

(b)

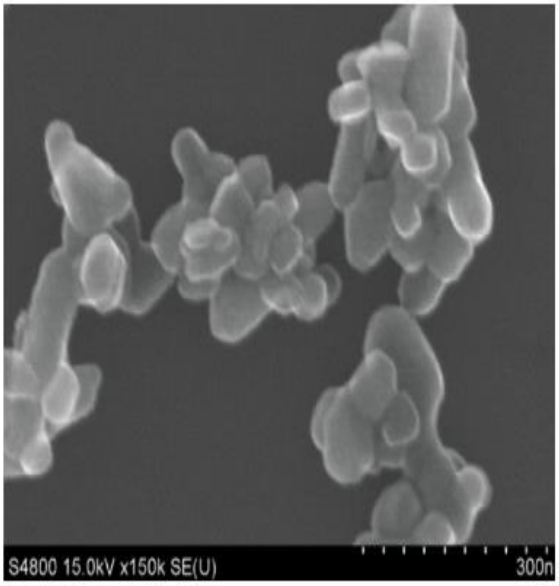

(c)

Journal of Science and Technology
ISSN: 2456-5660, Volume 6, Issue 6 (NOV-DEC 2021)

www.jst.org.in DOI: https://doi.org/10.46243/jst.2021.v6.i6.pp19-30

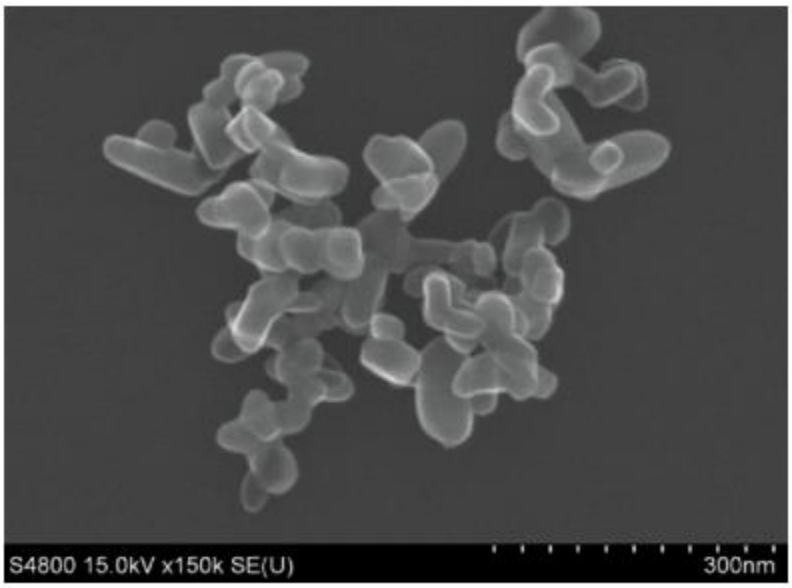

(d)

SEM images of TiO2 NPs are shown in Figure 1. A1 TiO2 NPs have a diameter of 45:87 7:75 nm. Its diameter is 79:39 to 22:58nm for A2 TiO2 nanoparticles. (b) In terms of size, the R1 TiO2 NPs had a diameter and length of 52:37 nm and 86:55 nm, respectively. (d) R2 TiO2 NPs have a diameter of 25:46 nm and a length of 75:34 nm. s. Staining of Mineralized Nodules. Cell mineralization in MC3T3-E1 cells was studied using Alizarin Red S staining. An osteogenic medium comprised of MEM medium, 10 mmol/L beta-glycerophosphate, and 0.05 mmol/L ascorbic acid was used to expose the cells to four different kinds of TiO2 nanoparticles. Every three days, the osteogenic media was replaced. After 28 days, the cell layers were rinsed three times with PBS and fixed in 95 percent ethanol for 10 minutes, as shown in Figure 1. The cells were then stained for 30 minutes with 0.1 percent Alizarin Red S after three washes with water. Images and counts of the mineralized nodules were obtained using microscopy. Analysis of statistical data. The SPSS 13.0 statistical software was used to examine all of the data (SPSS Inc., USA). One-way analysis of variance was used to analyse the experimental data (ANOVA). Results with a p-value of 0.05 or less were deemed significant..

Results

3.1. TiO2 NP characterization. A detailed description of both anatase and rutile TiO2 was supplied and described. Figures 1 and 2 show images of TiO2 NPs taken under SEM and TEM conditions. Figure 1(a) shows that the anatase TiO2 A1 had an average diameter of 45:87 7:75 nm, similar to that of red blood cells (Figure 2(a)). For A2, we found that it had an average diameter of 79:39 nm (Figure 1a). R1 and R2 were long rods of various diameters for the rutile TiO2 (Figures 2(c) and 2(d)). As shown in Figure 1(c), the average length and diameter of R1 were 86:55 nm and 52:37 nm, respectively. For R2, these values were 75:34 nm and 13:28 nm, respectively (Figure 1(d)). Table 1 summarises and lists the physical parameters of TiO2 NPs. In order to study the aggregation of TiO2 NPs in solution, DLS was applied. Figure 3 shows the distribution of TiO2 NPs' hydrodynamic diameters in an aqueous solution. Rutile TiO2 revealed a peak at 408 7.7 nm (size distribution from 141 to 1106 nm) with a Zeta potential of 2.3 mV, suggesting that R1 was readily agglomerated and aggregated in solution. Due to the R2 suspension's zeta potential value of -22.0 mV, the R2 peak at 183.6 nm (size distribution from 105 to 396 nm) indicated that the R2 suspension was stable (Table 1). It was found that anatase A1 had an average diameter of 166.6 nm, whereas A2 had a high peak of 235.3 nm and a lower peak of 5.01 nm. Table 1 lists the zeta potentials of the anatase and rutile

www.jst.org.in DOI: https://doi.org/10.46243/jst.2021.v6.i6.pp19-30

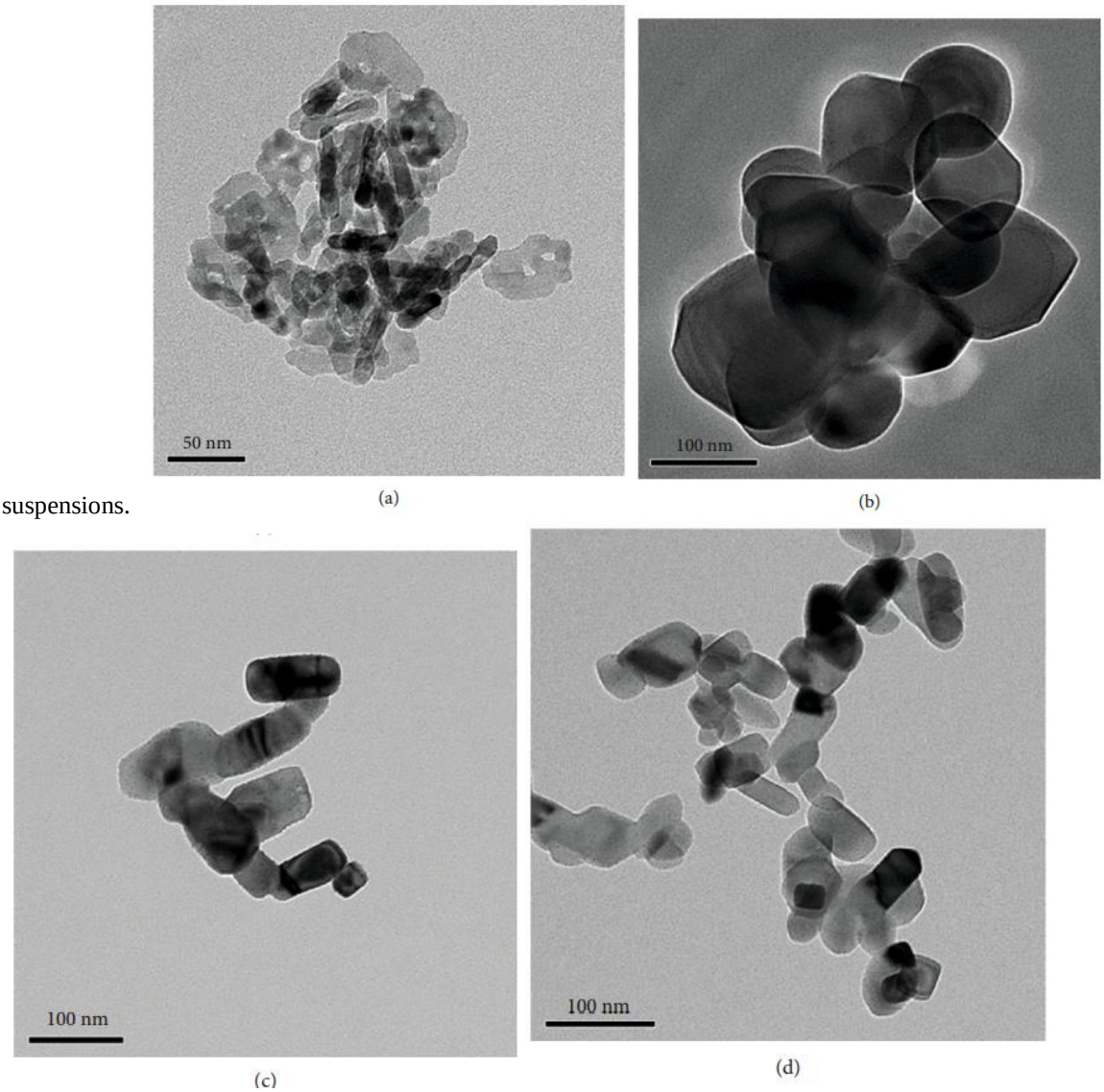

suspensions.

Figure 2: Micrographs of TiO2 NPs by TEM: (a) A1 is erythrocyte like; (b) A2 is spherical; (c) R1 is a long rod; (d) R2 is a long rod.

3.2.Determination of TiO2 NP Concentration.

Using a camera to film the TiO2 NPs sedimentation, we were able to determine the concentration of the NPs to utilise. Figure S1 illustrates the 12-hour sedimentation of TiO2 in PBS containing BSA at concentrations of 10, 30, and 100 g/mL. After two hours of standing, the 100 g/mL TiO2 NP group was allowed to settle. Flocculated precipitations were seen after 12 hours of incubation with TiO2 NPs in the presence of 30 g/mL TiO2 NPs. After settling for 12 hours at a concentration of 10 g/mL, no sediment was found in the suspension. In PBS and culture media for 48 hours, TiO2 NPs lower than 30 g/mL sedimented in Figure S2. As a reference, we used culture media containing 20 g/mL TiO2 NPs as a control. Precipitates were observed in the 30 g/mL group 12 h after incubation, however no precipitates were identified in the TiO2 NPs less than 20 g/mL after 48 h. Both in PBS and in culture media, a suspension of less than 20 g/mL demonstrated excellent stability and dispersion. MC3T3-E1 Cell Viability (3.3) TiO2 NPs were added to the culture. Different concentrations of A1 and R2 TiO2 NPs in MC3T3-E1

www.jst.org.in DOI: https://doi.org/10.46243/jst.2021.v6.i6.pp19-30

preosteoblast cells were used to measure cell viability (Figure 4). After 24 hours of incubation, cell viability was reduced by more than 50% when the concentration of TiO2 NPs exceeded 50 g/mL (Figure 4(a)). TiO2 NPs concentrations between 30 and 50 g/mL substantially decreased cell viability compared to the control group (Figure 4(c)). Cell viability was unaffected by TiO2 NP concentrations lower than 10 g/mL (Figure 4(b)). TiO2 NPs are similarly effective at 20 g/mL.

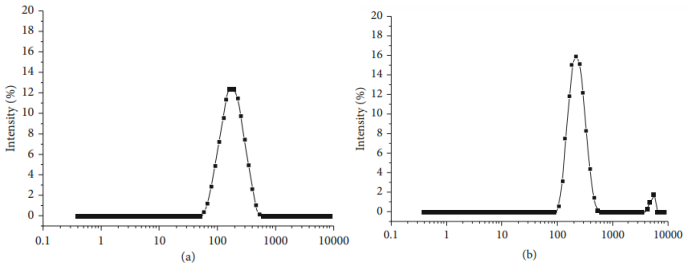

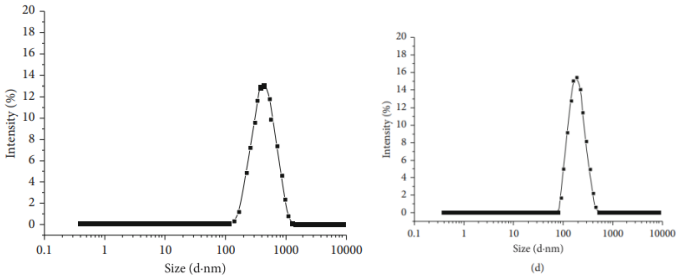

Using the DLS approach, we determined the hydrodynamic diameter distribution of nano-TiO2 in water. (a) A1 has a maximum diameter of 166.6 nm on average. In (b), A2 displays an extremely high, narrow peak at 235.3 nm. At 408.7 nanometers, R1 exhibits a peak. Cell survival was unaffected by R2's small peak at 183.6 nm. TiO2 NPs were found to be cytotoxic at concentrations above 20 g/mL, according to these results, which indicated a critical threshold for cell viability. 3.4. MC3T3-E1 Cells Express ALP and OCN. The MC3T3-E1 cells were cocultured with A1 and R1 TiO2 NPs at concentrations of 20, 50, and 100 g/mL for 7 and 14 days to examine the effect of NPs on ALP expression. The osteogenic differentiation capacity of all experimental groups was dramatically reduced in comparison to the blank control group (Figure 5(a)). Furthermore, A1 and R1 TiO2 NPs had varied effects on osteoblast differentiation, depending on the concentration. R1's inhibitory impact on cell differentiation is less than A1's at low concentrations. While anatase and rutile materials had similar inhibitory effects on cell differentiation, as NP concentration increased, rutile materials were more effective in inhibiting cell differentiation. Figure 5 depicts the 14-day ALP levels of cells cocultured with A1 and R1 materials (b). In comparison to the control, the ALP level decreased by 64.30% when A1 concentration was 20 ng/mL. The ALP level reduced by 43.01 percent and 47.69 percent when the concentration was 50 and 100 g/mL, respectively. R1 had a comparable impact on cell differentiation to A1 in terms of inhibiting cell proliferation. A1 and R1 were shown to have a detrimental effect on preosteoblast cell development. Of course, the experiment groups and the control group did not vary significantly when it came to OCN findings (Figure S3). Assessment of ROS Production and Antioxidant Level 3.5 ROS generation has been implicated with TiO2 NP toxicity in several studies. Figure 6 shows the findings of the ROS generation and antioxidant levels in MC3T3-E1 cells examined in this research. TiO2 NP treatment enhanced the fluorescence of oxidised DCF in cells (Figure 6(a)), particularly in the A1, R1, and R2 groups (p 0:05). Figure 6. This indicated that the treatment with 20 g/mL TiO2 NPs created ROS. It was also possible to measure cell superoxide generation using WST 1. Four different varieties of TiO2 NPs produced considerably more superoxide

www.jst.org.in DOI: https://doi.org/10.46243/jst.2021.v6.i6.pp19-30

when compared to the control group (Figure 6(b)). The primary glutathione (T-GSH)

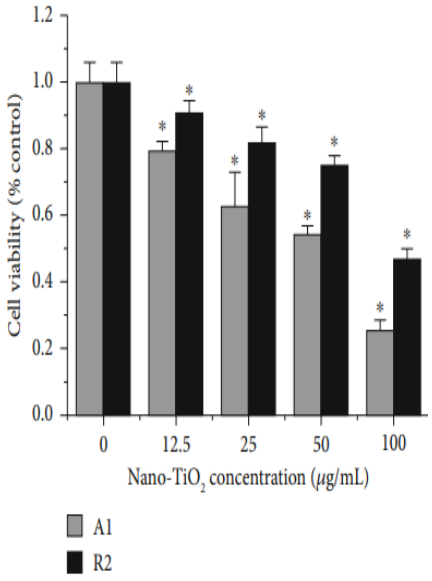

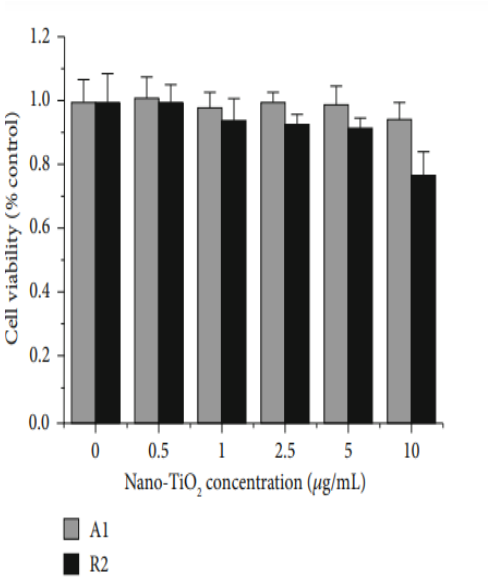

www.jst.org.in DOI: https://doi.org/10.46243/jst.2021.v6.i6.pp19-30

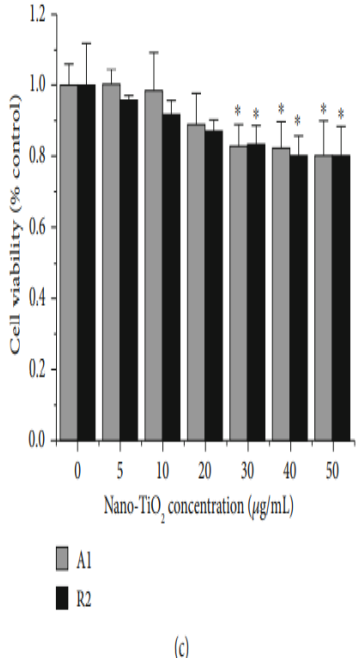

Figure 4: Cell viability of MC3T3-E1 cells cocultured with different concentrations of TiO2 NPs. ∗p < 0:05 significantly different from the corresponding control group

The A1 and R1 groups had considerably reduced levels of T-GSH (Figure 6(c)). MC3T3-E1 cells were also found to have high levels of SOD and MDA, which indicated oxidative stress. Figures 6(d) and 6(e) show that SOD and MDA activity was marginally greater in the TiO2 NP-treated group than in the control group (p 0:05) after the treatment (Figures 6(d) and 6(e)). The TEM is at 3.6. MC3T3-E1 Cell Characterization TiO2 NPs were added to the culture. The membrane of MC3T3-E1 cells was deformed and caved in after coculturing with TiO2 NPs, enclosing the aggregated TiO2 NPs. TiO2 NPs were shown to be grouped around the nucleus inside the plasma membrane of cells (Figure 7(b)). This ultrastructural alteration was triggered by the internalisation of TiO2 NPs, some of which were found in the mitochondria of MC3T3-E1 cells. Although the nucleus was clearly visible, the nuclear envelope was deformed. The nuclear chromatin was in the meanwhile compressed and dispersed throughout the nucleus' periphery. It was shown that when the number of mitochondria and lysosomes rose, the lamellar cristae began to become more irregular. At the same time, the architecture of mitochondria were inflated and void, indicating that the organelle had been damaged by the storage of nano-TiO2. The enlargement of the golgi complex (Figure 7(c)) further revealed that the golgi complex had been damaged. Disintegration and an apoptotic body formed after exposure to A2 and R2 for 24 hours (Figures 7(d) and (e)). Because of their absorption into cells and subsequent subcellular damage, TiO2 nanoparticles were shown to be toxic according to TEM analysis. This section focuses on

cell death and mineralization in MC3T3-E1 cells TiO2 NPs were added to the culture. Apoptosis and necrosis in

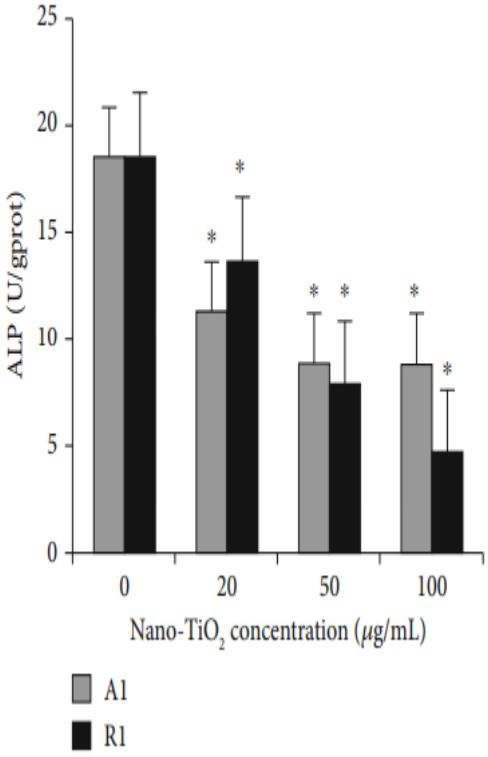

MC3T3-E1 cells were detected by flow cytometry.

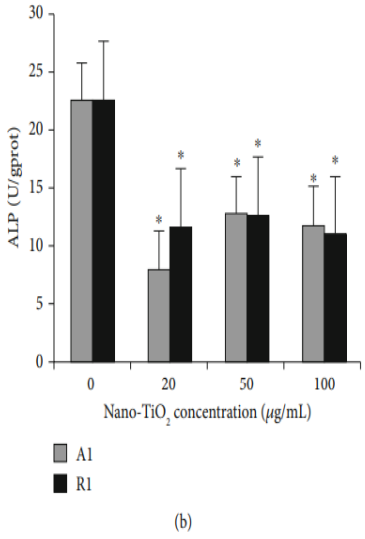

(b)

Conclusion

Bone formation is negatively affected by TiO2 NPs. Nano-TiO2 concentrations, geometries, and coculture periods all affect bone cell proliferation and differentiation in distinct ways, as seen below. According to a general rule,

nano-TiO2 in tissues may lead to a reduction in osteoblast activity as well as blocked bone formation if the presence of nano-TiO2 is present.

References

[1] J. Jeevanandam, A. Barhoum, Y. S. Chan, A. Dufresne, and M. K. Danquah, "Review on nanoparticles and nanostructured materials: history, sources, toxicity and regulations," Beilstein Journal of Nanotechnology, vol. 9, pp. 1050–1074, 2018.

[2] H. Shi, R. Magaye, V. Castranova, and J. Zhao, "Titanium dioxide nanoparticles: a review of current toxicological data," Particle and Fibre Toxicology, vol. 10, no. 1, p. 15, 2013.

[3] S. Silva, H. Oliveira, A. M. S. Silva, and C. Santos, "The cytotoxic targets of anatase or rutile + anatase nanoparticles depend on the plant species," Biologia Plantarum, vol. 61, no. 4, pp. 717–725, 2017.

[4] A. Hasan, M. Morshed, A. Memic, S. Hassan, T. Webster, and H. Marei, "Nanoparticles in tissue engineering: applications, challenges and prospects," International Journal of Nanomedicine, vol. Volume 13, pp. 5637–5655, 2018.

[5] X. Li, J. Wei, K. E. Aifantis et al., "Current investigations into magnetic nanoparticles for biomedical applications," Journal of Biomedical Materials Research Part A, vol. 104, no. 5, pp. 1285–1296, 2016.

[6] A. Jimeno-Romero, M. Oron, M. P. Cajaraville, M. Soto, and I. Marigomez, "Nanoparticle size and combined toxicity of TiO2 and DSLS (surfactant) contribute to lysosomal responses in digestive cells of mussels exposed to TiO2 nanoparticles," Nanotoxicology, vol. 10, no. 8, pp. 1168–1176, 2016.

[7] T. H. Kim, M. S. Kang, N. Mandakhbayar, A. El-Fiqi, and H. W. Kim, "Anti-inflammatory actions of folatefunctionalized bioactive ion-releasing nanoparticles imply drug-free nanotherapy of inflamed tissues," Biomaterials, vol. 207, pp. 23–38, 2019.

[8] I. Pujalte, D. Dieme, S. Haddad, A. M. Serventi, and M. Bouchard, "Toxicokinetics of titanium dioxide (TiO2) nanoparticles after inhalation in rats," Toxicology Letters, vol. 265, pp. 77–85, 2017.

[9] S. Vial, R. L. Reis, and J. M. Oliveira, "Recent advances using gold nanoparticles as a promising multimodal tool for tissue engineering and regenerative medicine," Current Opinion in Solid State & Materials Science, vol. 21, no. 2, pp. 92–112, 2017.

[10] K. Zhang, Y. Fan, N. Dunne, and X. Li, "Effect of microporosity on scaffolds for bone tissue engineering," Regenerative Biomaterials, vol. 5, no. 2, pp. 115–124, 2018.

[11] A. J. Haider, Z. N. Jameel, and I. H. M. Al-Hussaini, "Review on: titanium dioxide applications," Energy Procedia, vol. 157, pp. 17–29, 2019. [12] M. H. Hamzah, S. Eavani, and E. Rafiee,"CoAl2O4/TiO2 nano composite as an anti-corrosion pigment," Materials Chemistry and Physics, vol. 242, p. 122495, 2020.

[13] I. Narkevica, L. Stradina, L. Stipniece, E. Jakobsons, and J. Ozolins, "Electrophoretic deposition of nanocrystalline TiO2 particles on porous TiO2-X ceramic scaffolds for biomedical applications," Journal of the European Ceramic Society, vol. 37, no. 9, pp. 3185–3193, 2017.

[14] T. V. S. S. P. Sashank, B. Manikanta, and A. Pasula, "Fabrication and experimental investigation on dye sensitized solar cells using titanium dioxide nano particles," Materials Today: Proceedings, vol. 4, no. 2, pp. 3918–3925, 2017.

[15] J. Ferin, G. Oberdörster, and D. P. Penney, "Pulmonary retention of ultrafine and fine particles in rats," American Journal of Respiratory Cell and Molecular Biology, vol. 6, no. 5, pp. 535– 542, 1992.

[16] R. Kumazawa, F. Watari, N. Takashi, Y. Tanimura, M. Uo, and Y. Totsuka, "Effects of Ti ions and particles on neutrophil function and morphology," Biomaterials, vol. 23, no. 17, pp. 3757–3764, 2002.

[17] T. Brzicova, J. Sikorova, A. Milcova et al., "Nano-TiO2 stability in medium and size as important factors of toxicity in macrophage-like cells," Toxicology In Vitro, vol. 54, pp. 178– 188, 2019.

[18] M. Ibrahim, J. Schoelermann, K. Mustafa, and M. R. Cimpan, "TiO2 nanoparticles disrupt cell adhesion and the architecture of cytoskeletal networks of human osteoblast-like cells in a size dependent manner," Journal of Biomedical Materials Research Part A, vol. 106, no. 10, pp. 2582–2593, 2018.

[19] K. Hattori, K. Nakadate, A. Morii, T. Noguchi, Y. Ogasawara, and K. Ishii, "Exposure to nano-size titanium dioxide causes oxidative damages in human mesothelial cells: the crystal form rather than size of particle contributes to cytotoxicity," Biochemical and Biophysical Research Communications, vol. 492, no. 2, pp. 218–223, 2017.

[20] M. J. Bessa, C. Costa, J. Reinosa et al., "Toxicity of rutile TiO2 nanoparticles immobilized in nanokaolin nanocomposites on HepG2 cell line," Toxicology and Applied Pharmacology, vol. 316, pp. 114–122, 2017.